

Reservoir Computing with Dipole-Coupled Nanomagnets



Hikaru Nomura, Hitoshi Kubota, and Yoshishige Suzuki

Abstract An idea to use a magnetic nano-dots array for a reservoir computing is introduced. The mechanism of how the nonlinear calculation is carried out in the magnetic system is explained by showing the simplest case with three nano-dots system. The first trial to prove calculation ability and fabrication ability of the system is demonstrated. Since the proposed reservoir computing system may utilize integration technology of the magnetic random access memory (MRAM), it possesses a possibility to realize a large-scale reservoir computing system.

1 Spin-Glass Model and Spin-Glass Reservoir Computing

The Hopfield model (Hopfield 1982) and the Boltzmann machine (Ackley et al. 1985) are well-known mathematical models of recurrent neural networks (RNN). They are based on a physical model of magnetic material with randomness (Amit and Gutfreund 1985) called a spin glass. Classical view of the spin is a rotation of the electron itself that causes magnetic moment of the atoms. In a spin glass,

H. Nomura · Y. Suzuki (✉)

Graduate School of Engineering Science, Osaka University, Machikaneyama 1-4, Toyonaka, Osaka 560-8531, Japan

e-mail: suzuki-y@mp.es.osaka-u.ac.jp

Center for Spintronics Research Network, Osaka University, Machikaneyama 1-4, Toyonaka, Osaka 560-8531, Japan

H. Nomura

e-mail: nomura@mp.es.osaka-u.ac.jp

H. Nomura

Graduate School of Engineering, Osaka University, Yamada-oka 1-1, Suita, Osaka 565-0871, Japan

H. Kubota

National Institute of Advanced Industrial Science and Technology (AIST), 1-1-1 Umezono, Tsukuba, Ibaraki 305-8568, Japan

each atom acts as a magnet and interacts with each other via a quantum mechanical exchange interaction, J . In terms of neural concepts, the direction of magnetic dipole moment of an atom can be considered as the electrochemical potential of a neuron and the interaction J as the synaptic weight. Thus, magnetic materials can be treated as models of RNN and sophisticated techniques from statistical physics can be applied to analyze RNNs. In particular, the “infinite range model” (Fig. 1), where an infinite number of atoms (neurons/nodes) with all inter-atomic exchange interactions (inter-neuron/inter-node connections), is considered, which simplifies the problem tremendously because the mean-field approximation from statistical physics can provide an exact solution for the model. In addition, the Ising spin model, in which the direction of the magnetic moment is constrained along $+z$ - or

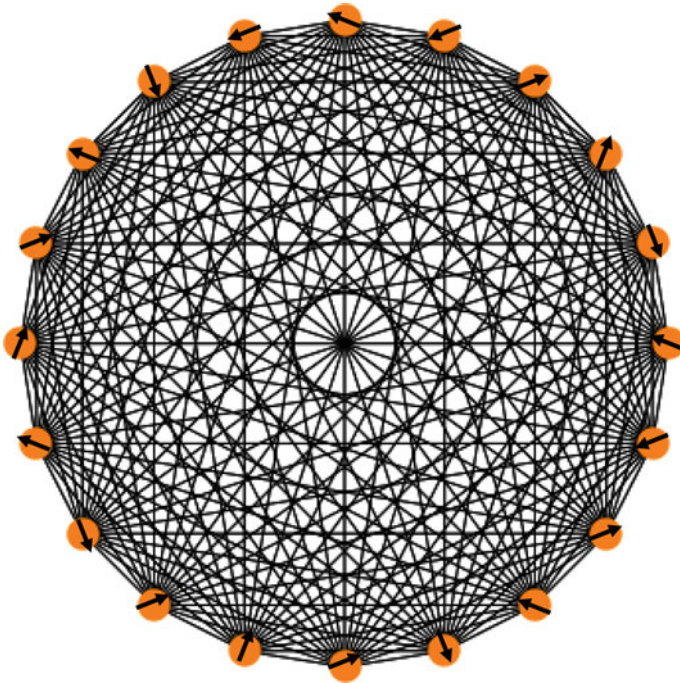


Fig. 1 Infinite range model of a spin glass. Orange disks are atoms with magnetic momentum vectors (arrows). Black lines express exchange interactions, J , between two atoms. Depending on the sign of J , connected two magnetic moments prefer parallel or antiparallel configurations. Since all atoms are connected by lines, the model is regarded as an “infinite range model.” This is an idealization of the real spin glass, in which the atoms align in a solid and the exchange interactions are limited between neighboring atoms. In terms of neuromorphic computation, the atoms represent neurons (nodes), and lines represent axons/synapses complex (undirected inter-connections and synaptic weights). In the spin-glass system, because of a randomness in the atom positions, J is distributed. As a consequence, the system has many energy minima. This means that the system has many quasi-equilibrium states with complicated alignments of magnetic moments. In this chapter, we aim to use such a system as a reservoir

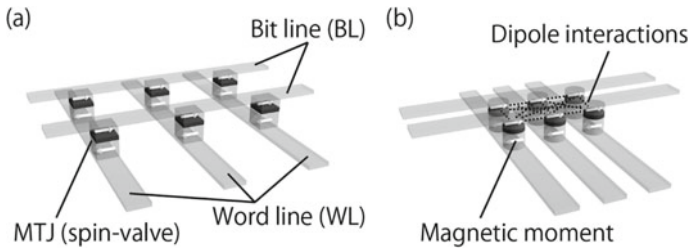


Fig. 2 **a** MRAM. The MRAM comprises magnetic tunnel junctions (MTJs) and selection transistors underneath (not shown). As an example, the MTJ can have a magnetic free layer of $20 \text{ nm} \times 20 \text{ nm} \times 2 \text{ nm}$. The direction of the magnetic moment in the free layer, which is illustrated by the white arrow in the black layer, corresponds to one bit of binary information. Since the resistance of the MTJ depends on the relative angle between the free layer magnetic moment and the reference layer (white arrow in the gray color layer) (Yuasa et al. 2004; Parkin et al. 2004), one may read out individual bit information electrically. **b** Magnetic reservoir made of MTJ array. The magnetic dipole interaction between the magnetic free layers allows linear/nonlinear operations among the stored information and makes the system an effective reservoir

$-z$ -directions, can also simplify the problem without losing its essential calculation ability. These generalizations and simplifications of the spin-glass model resulted in the Hopfield model and Boltzmann machine.

Therefore, one may expect that magnetic materials can serve as good natural systems to realize RNNs. However, limited researches have been done to produce RNNs using the spin glasses. This is because individual atomic magnets cannot be easily controlled. On the other hand, recent developments in the field of electronics have made it possible to integrate large numbers of nano-sized magnets (hereafter called “nanomagnets”) to construct a solid-state magnetic random access memory (MRAM) (Bhatti et al. 2017) (Fig. 2a). In MRAM, one may read out each bit information, which is stored as the direction of the magnetic moment in a cell, using the magnetoresistive effect (Yuasa et al. 2004; Parkin et al. 2004). The cell is called as a magnetic tunnel junction (MTJ), in which the resistance is dependent on the relative angle between two magnetic dipole moments in the junction, i.e., of free layer and reference layer. One may also write-in the information by applying either a current (Myers et al. 1999) or a voltage (Maruyama et al. 2009). To construct a stable memory, the interaction between the nanomagnets is removed in the MRAM. In contrast, here, we intentionally use the interaction between the nanomagnets to allow the MRAM to work as a spin-glass system and perform as an RNN. Since nanomagnets are electronically separated in the MRAM, the exchange interaction between the cells does not exist. However, magnetic dipole interaction exists that allows nanomagnets to perform linear/nonlinear calculations, as it will be explained later in this chapter (Fig. 2b). The strengths of the magnetic dipole interactions are determined from the size of magnetic dipole moments and distance between the magnets. Therefore, they cannot be modified after the device has been fabricated. This means that the system can be considered as an RNN with fixed synaptic weights.

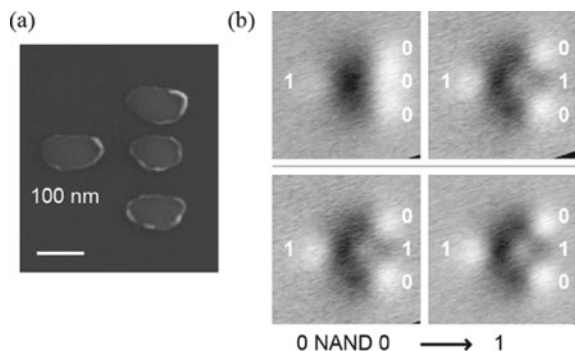
As a consequence, the framework of reservoir computing (Jaeger and Haas 2004) is needed to perform machine learning.

As magnetic systems have rich dynamics, usage of dynamic states can increase the performance of magnetic reservoirs. For example, spin-torque oscillators offer a relatively high performance when used as a reservoir working at high frequency (see the chapters by Grollier and Tsunegi). In this chapter, we show that static magnetic systems have also shown relatively high performance by increasing the number of nanomagnets. In particular, we show that the voltage control of magnetic anisotropy (VCMA) offers a way to realize a large-scale, high-performance, and energy-efficient magnetic RNN.

2 Historical Design of the Magnetic Boolean Calculator

A Boolean operation element using dipole-coupled nanomagnets is called a nanomagnet logic (NML) (Cowburn and Welland 2000). NML comprises nanomagnets with single magnetic domain states. The binary state is defined by the polarity of the magnetic moment of the nanomagnet that is similar to MRAM. The nanomagnets communicate each other via dipole interaction. The magnetic moment of a nanomagnet aligns parallel to the stray field from surrounding nanomagnets. Since the direction of the stray field is determined by the major polarity of the surrounding magnets, the NML gate is basically a majority gate. A transmission line (Cowburn and Welland 2000), a NAND/NOR gate (Imre et al. 2006; Hikaru and Ryoichi 2011), a shift register (Hikaru et al. 2017), etc. have been previously realized (Orlov et al. 2008). Figure 3a, b shows a scanning electron microscope (SEM) image of the NML-NAND/NOR logic gate (Hikaru and Ryoichi 2011) and magnetic force microscope images of a typical operation results, respectively. Until now, NMLs have been designed to perform only Boolean operations. However, if the analog value of the magnetic moment vector is used, the NML becomes an attractive candidate for a physical reservoir.

Fig. 3 **a** SEM image of the NML NAND/NOR gate. **b** Magnetic force microscope images of a typical operation of the NML NAND/NOR gate (Hikaru and Ryoichi 2011)



3 Linear and Nonlinear Calculation Using Nanomagnets

The energy (Hamiltonian: H) of a single nanomagnet with uniaxial anisotropy under an external magnetic field is written as follows:

$$\begin{cases} H = -\frac{1}{|\vec{M}|^2} \vec{M}^t \hat{K} \vec{M} - \mu_0 \vec{M} \cdot \vec{H}_{ext} \\ \hat{K} = K_u V \begin{pmatrix} 0 & 0 & 0 \\ 0 & 0 & 0 \\ 0 & 0 & 1 \end{pmatrix} \end{cases}, \tag{1}$$

where \vec{M} is the magnetic moment vector, \hat{K} is the anisotropy tensor, $K_u > 0$ is the uniaxial anisotropy energy par unit volume, V is the volume of the nanomagnet, μ_0 is the magnetic susceptibility of vacuum, and \vec{H}_{ext} is the external magnetic field vector. If we can neglect formation of a magnetic domain inside the nanomagnet, the size of the magnetic moment, $|\vec{M}|$, is the constant whereas it may change the direction. Here, we assumed a disk-like nanomagnet, where the z -axis is perpendicular to the plane of the disk (Fig. 4a). Note that \vec{M} is stable if its direction minimizes H .

In Fig. 4b, the magnetic hysteresis curves for an external field parallel to $\vec{e}_x + \vec{e}_z$ (45° from the normal line of the disk) are shown. The solid and dotted curves show the x - and z -components of \vec{M} , respectively. When there is no external field, because of the uniaxial magnetic anisotropy, there are two equilibrium points, which are indicated as (i) and (i') in Fig. 4b, i.e., $\vec{M} = \pm M \vec{e}_z$, where \vec{e}_z is the unit vector in the

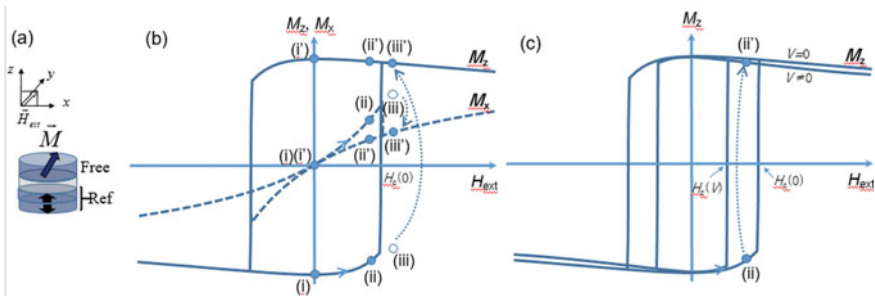


Fig. 4 **a** Schematic diagram of MTJ with perpendicular anisotropy. The free and reference layers are made of ferromagnetic materials and are separated by an insulator layer such as MgO. Employing a very thin insulator (about 1 nm), one may get a tunneling current through the insulator that is dependent on the relative angle between the two magnetic moments at both sides of the insulator layer. To avoid a stray magnetic field from the reference layer, the reference layer comprises two magnetic layers with opposite magnetic moments. **b** Magnetic moment as a function of external magnetic field, which is applied at an angle of 45° from the symmetrical axis of the MTJ. Further details are provided in the text. **c** Application of a voltage on the MTJ reduces the magnetic anisotropy energy and coercive force, H_c , through the VCMA

z -direction. Now, we trace the hysteresis starting from a state with $\vec{M} = -M\vec{e}_z$. It means that the x - and z -components of \vec{M} are 0 and $-M$, respectively (Fig. 4b (i)). When the external magnetic field increases, \vec{M} begins to tilt toward the x -direction. Therefore, both M_x and M_z increase (Fig. 4b (ii)). Here, although the energy at point (ii') is smaller than that at point (ii), the state remains at point (ii), which corresponds to a local minimum in the Hamiltonian. When the magnetic field reaches the coercive force, H_c , the saddle point that separates the two minima disappears. Then, the state does not stay at (iii) but jumps to (iii'). As a consequence, M_z becomes positive and a small jump occurs for M_x . Although a small jump exists, we can assume that M_x is a sigmoid-like function of H_{ext} . In an array of nanomagnets, the magnetic field exerted on a nanomagnet is the sum of all dipole fields made by the other nanomagnets. Therefore, the nanomagnet calculates a sigmoid-like function of the sum of the dipole fields. Hence, the nanomagnet has a nonlinear calculation power. In contrast to M_x , M_z shows a large hysteresis. The jump from point (iii) to point (iii') corresponds to the firing of a neuron that has a certain threshold. After firing, the nanomagnet stores the information about the sign of the previous external magnetic field until another large external field is applied. Therefore, a nanomagnet has a memory function. In Fig. 4c, the effect of voltage application on the hysteresis curve is shown. The application of a voltage reduces the magnetic anisotropy and correspondingly reduces the coercive force, H_c . As a consequence, state at point (ii) may jump to point (ii'). By using these phenomena, the information about the sum of the dipole fields can be written to the nanomagnet.

The Hamiltonian of an array of nanomagnets is written as follows:

$$H_{array} = \mu_0 \left(- \sum_{i,j} \vec{M}_i^t \hat{J}_{ij} \vec{M}_j - \sum_i \vec{H}_{ext} \cdot \vec{M}_i \right)$$

$$\hat{J}_{ij} \equiv \begin{cases} \frac{\hat{K}_i}{\mu_0 |\vec{M}_i|^2}; & i = j \\ \frac{1}{2} \hat{D}_{dipole,ij}; & i \neq j \end{cases}, \quad (2)$$

where

$$\left\{ \begin{array}{l} \hat{K}_i = K_{u,i} V_i \begin{pmatrix} 0 & 0 & 0 \\ 0 & 0 & 0 \\ 0 & 0 & 1 \end{pmatrix} \\ \hat{D}_{dipole,ij} = \frac{1}{4\pi r_{ij}^5} \begin{pmatrix} 3r_{x,ij}^2 - r_{ij}^2 & 3r_{x,ij}r_{y,ij} & 3r_{x,ij}r_{z,ij} \\ 3r_{x,ij}r_{y,ij} & 3r_{y,ij}^2 - r_{ij}^2 & 3r_{y,ij}r_{z,ij} \\ 3r_{x,ij}r_{z,ij} & 3r_{y,ij}r_{z,ij} & 3r_{z,ij}^2 - r_{ij}^2 \end{pmatrix} \\ \vec{r}_{ij} = \vec{r}_j - \vec{r}_i = \begin{pmatrix} r_{x,ij} \\ r_{y,ij} \\ r_{z,ij} \end{pmatrix}. \end{array} \right. \quad (3)$$

Here, \vec{M}_i , \hat{K}_i , $K_{u,i}$, and V_i are the magnetic moment vector, anisotropy tensor, uniaxial anisotropy energy per unit volume, and volume of the nanomagnet at site i , respectively. $\hat{D}_{dipole,ij}$, and \vec{r}_{ij} are the dipole matrix, and relative position vector at site i with respect to a nanomagnet at site j , respectively.

By observing the first line in Eq. (2), one may find that the Hamiltonian is similar to that of the spin glass although it is a classical Hamiltonian with dipole interaction.

From Eq. (2), one can obtain effective magnetic field, $\vec{H}_{effect,k}$, exerted on the k th nanomagnet as follows:

$$\begin{aligned} \vec{H}_{effect,k} &= -\frac{1}{\mu_0} \frac{\partial H_{array}}{\partial \vec{M}_k} \\ &= \vec{H}_{ani,k} + \sum_{i \neq k} \vec{H}_{dipole,ki} + \vec{H}_{ext} \end{aligned} \quad (4)$$

where,

$$\begin{aligned} \vec{H}_{ani,k} &= \frac{2}{\mu_0} \frac{\hat{K}_k}{|\vec{M}_k|^2} \vec{M}_k : \text{Anisotropy field} \\ \vec{H}_{dipole,ki} &= \hat{D}_{dipole,ki} \vec{M}_i : \text{Dipole field} \end{aligned}$$

The effective field is a sum of anisotropy field, dipole field, and external field. The k th magnetic moment is stable if it is parallel to the effective field at the site. Therefore, it may calculate a sigmoid-like function of the sum of those fields.

A schematic diagram of a dipole magnetic field around a nanomagnet is shown in Fig. 5a. Because of the field, two nanomagnets with perpendicular magnetic moments couple antiparallel with each other when the dipole field is smaller than the anisotropy field. Under large dipole fields, the magnetic moments turn to in-plane and align parallel to the line that connects the two nanomagnets. If there are three nanomagnets on a plane, e.g., at the vertices of an equilateral triangle (see Fig. 5b), ‘‘frustration’’ happens. Then, for a large dipole field, all the magnetic moments turn into the plane and align circularly; this is called the vortex state.

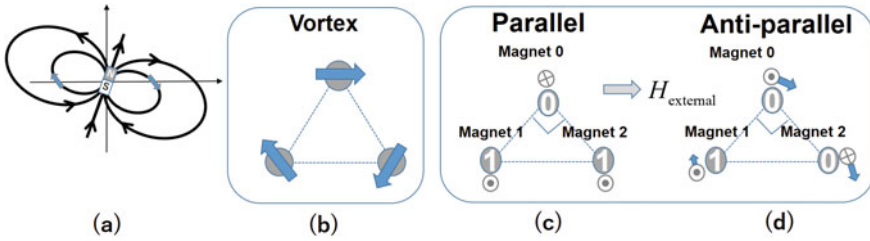


Fig. 5 **a** Magnetic dipole field distribution around a nanomagnet. **b** A system with three nanomagnets, which are placed at the vertices of an equilateral triangle. **c** A system with three nanomagnets, where the magnetic moments of magnets 1 and 2 are parallel. **d** A system with three nanomagnets, where the magnetic moments of magnets 1 and 2 are antiparallel. Here, magnets 1 and 2 are used for the input of information and magnet 0 is used for the output. The values 0 and 1 correspond to the magnetic moments in the $-z$ - and $+z$ -directions, respectively. The arrows beside the disk represent the magnetic moment vectors

Now, we discuss a realistic case that employs a system with three nanomagnets (see Fig. 5c, d). Three nanomagnets are placed on a plane and arranged at the vertices of an isosceles right triangle. A small magnetic field toward $+x$ -direction is applied to break the time-reversal symmetry (see Fig. 5). For this model, we can find a stable set of $\{\vec{M}_i\}$ by finding the minima in H_{array} . Figure 5c, d shows two stable alignments of the magnetic moments. The z and in-plane components of the magnetic moments are also shown. Here, as for an example, we employ nanomagnets with radius, thickness, and saturation magnetization as 20 nm, 2 nm, and 1.3 MA/m, respectively. Magnetic anisotropy field for perpendicular magnetization without voltage application is about 3.1 mT (2.5 kA/m). Distance between magnet 1 and 2 is $50 \times \sqrt{2}$ nm. In Fig. 5c, the magnetic moments of both magnets 1 and 2 point toward the $+z$ -direction, which corresponds to the “1” state. As a consequence, the magnetic moment of magnet 0 points toward the $-z$ -direction (“0” state) because of dipole coupling. The state is obtained using the following protocol. First, the magnetic moments of magnets 0, 1, and 2 are set to point toward the $+x$ -, $+z$ -, and $+z$ -directions, respectively. Then, the system is relaxed to find a minimum in H_{array} near the initial state. After relaxation, a voltage is applied to reduce the perpendicular anisotropy of magnet 0. The voltage is increased slowly compared with the relaxation time to keep the system at the energy minimum. After reaching zero anisotropy, the voltage is slowly removed until it becomes zero. Using this protocol, the information about the dipole field at the position of magnet 0 is written to magnet 0. The alignment shown in Fig. 5c is natural because the distances between magnets 0 and 1 and magnets 0 and 2 are smaller than that of magnets 1 and 2. Figure 5d shows a case where the magnetic moments of magnets 1 and 2 are almost antiparallel. For this case, the frustration of the system makes the perpendicular magnetic moments unstable and all the moments tilt to make a vortex-like in-plane component. The magnetic moment of magnet 0 prefers the $+z$ -direction as a consequence of the delicate balance of the two dipole couplings and the external field.

Table 1 Normalized output of the system with three nanomagnets (Fig. 5b, c) and linear calculations between them. The system provides enough information to calculate AND, OR, and XOR functions using only linear calculus

$M_1 = a$	$M_2 = b$	$M_z = c$	$M_x = d$	AND = $\frac{1}{2}(a + b - d)$	OR = $\frac{1}{2}(a + b + d)$	XOR = d
0	0	1	0	0	0	0
0	1	-0.8	1	0	1	1
1	0	0.8	1	0	1	1
1	1	-1	0	1	1	0
$M_1 = a$	$M_2 = b$	$M_x = c$	AND = $\frac{1}{2}(a + b - c)$	OR = $\frac{1}{2}(a + b + c)$	XOR = c	
0	0	0	0	0	0	
0	1	1	0	1	1	
1	0	1	0	1	1	
1	1	0	1	1	0	

Without an external magnetic field, the time-reversed states are also stable and degenerate in energy. Note that, by time reversal, all the magnetic moments are reversed. With a small external magnetic field, the time-reversal symmetry is broken, and degeneracy of the time-reversed states is released. As a consequence, the time-reversed state of the antiparallel alignment of magnets 1 and 2 (Fig. 5d) is not stable. Instead, a state with reversed perpendicular moments and non-reversed in-plane moments with respect to the state shown in Fig. 5d becomes stable. The configurations of the magnetic moments of all the states are listed in Table 1. The 0 and 1 in the first and second columns represent the magnetic moments pointing toward the z - and $-z$ -directions, respectively. The third and fourth columns show the normalized values of the z - and x -components of the magnetic moment of magnet 0, respectively. By using those four values, results for the AND, OR, and XOR operations can be obtained using only linear calculus as shown in the fifth, sixth, and seventh columns of Table 1, respectively. This means that the system with three nanomagnets has linear/nonlinear calculation ability and can be used as a reservoir for reservoir computation. Note that such property based on the time-reversal breaking can be obtained without an external field if a system with four nanomagnets is employed. The breaking of the time-reversal symmetry can also be incorporated by taking into account magnetization dynamics with energy dissipation.

4 First Trial of the Dipole-Coupled Nanomagnet Reservoir

As for a first trial, an array system with $8 \times 8 \times 2$ (=128) nanomagnets was tested using a micromagnetic simulation. Figure 6a, b shows the schematic diagram of reservoir computing with dipole-coupled nanomagnet reservoir and the schematic

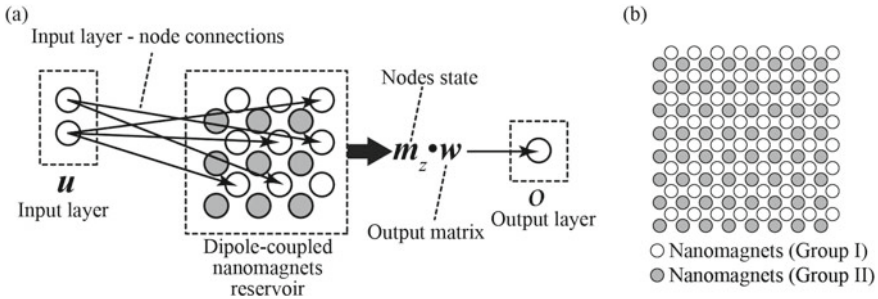


Fig. 6 **a** Schematic diagram of reservoir computing with dipole-coupled nanomagnets. **b** Schematic diagram of the top view of the reservoir with dipole-coupled nanomagnets

diagram of the top view of the reservoir with perpendicular magnetic anisotropy film, respectively. The radius and thickness of the nanomagnets were 20 nm and 0.3 nm, respectively. The gap between the nearest neighbor dots was 10 nm. The z -components of the normalized static magnetic moments of the nanomagnets were used as the state of the nodes denoted by m_z . The nodes (magnetic moments of the nanomagnets) are connected via magnetic dipole interactions. As mentioned previously, the static directions of the magnetic moments of the nanomagnets were determined from the previous direction of the magnetic moments and the dipole interaction between the entire nanomagnets in the reservoir. Therefore, the reservoir can be considered as a recurrent neural network. Some nodes were connected to the input layer u in the computer, and every nodes were connected to the output matrix w made in the computer. A dot product of the node state and the output matrix was stored in the output layer as the output of reservoir computing ($o = u \bullet w$). Binary and analog data were stored in the input layer and the output matrix, respectively.

First, when new data were set in the input layer, they were written to the input nodes (stage 1). To evaluate the system, as will be explained later, we randomly chose 48(=8 × 6) nodes from the 64 nodes of Group I (Fig. 6b) to be the input nodes and connected them to the input layer. The data in the input layer corresponding to the directions of magnetic moment were written using a writing method for MRAM. When the value in the input layer is 0/1, the direction of the magnetic moment of the input node is set to point toward the $-z/+z$ -direction.

Next, the state of the node was updated. To update the node state, we changed the magnetic anisotropy of the nanomagnet using the VCMA method. After writing the data to the input nodes, a bias voltage was applied to the Group II nanomagnets (stage 2) and then removed (stage 3). By applying an appropriate bias voltage to the nanomagnets, the magnetic anisotropy of the nanomagnets disappeared. With this change of magnetic anisotropy, the magnetic moments of the nanomagnets transitioned to the next state. During this transition, linear/nonlinear operations occurred as the directions of the magnetic moments of the nanomagnets changed.

The node state in stage 3 was connected to the output matrix. The node state (i.e., the z -components of the magnetic moments of the nanomagnets) was measured using

a reading method for MRAM (e.g., a reading method using tunneling magnetoresistive effect). A dot product of the node state and the output matrix was stored in the output layer using an external hardware. Then, a bias voltage was applied to the Group I nanomagnets (stage 4) and then removed (stage 5). The state of the node was updated by repeating the processes from stage 1 to stage 5.

In order to evaluate the behavior of the magnetic reservoir, we performed micro-magnetic simulations. We assumed that the nanomagnets take single-domain states and we used a single cell for a single nanomagnet in the simulations. The static direction of the magnetic moment was calculated by solving the Landau–Lifshitz–Gilbert (LLG) equation using the fourth-order Runge–Kutta method. The LLG equation at 0 K is as follows:

$$\frac{d\vec{M}_i}{dt} = -\gamma_{LL}\vec{M}_i \times \vec{H}_{eff,i} - \frac{\alpha\gamma_{LL}}{|\vec{M}_i|}\vec{M}_i \times (\vec{M}_i \times \vec{H}_{eff,i}), \quad (5)$$

α , γ_{LL} , and M_s are the damping constant, gyromagnetic ratio in the Landau–Lifshitz form, and saturation magnetization of the nanomagnets, respectively. The simulation parameters used were as follows: $\alpha = 0.5$, $\gamma_{LL} = 2.211/(1 + \alpha^2) = 1.7688$ m/As, and $|\vec{M}_i|/V_i = 1.3$ MA/m. Here, we employed large damping constant to shorten calculation time for the simulation. The large value of α employed here does not affect the following results since we only use static states for the RC. The typical value of the α is from 0.001 to 0.1 for metals.

We performed the NARMA10 task (Atiya and Parlos 2000) to evaluate the performance of the reservoir, which was previously to evaluate the performance of reservoirs (Appeltant et al. 2011; Nakajima et al. 2015). In the NARMA10 task, the output of step y_{s+1} is obtained from the previous inputs u_{s-k} and outputs y_{s-k} by the following equation:

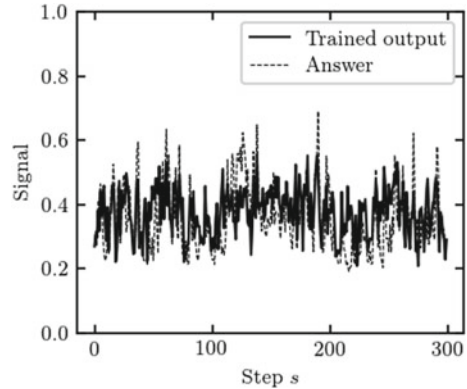
$$y_{s+1} = 0.3y_s + 0.05y_s \left(\sum_{k=0}^9 y_{s-k} \right) + 1.5u_s u_{s-9} + 0.1. \quad (6)$$

For the input u_s , random values ranging from 0 to 0.5 were used. The input data were normalized to an 8-bit unsigned integer before storing in the input layer. In each step, the 8-bit data was written to the 48 input nodes in the reservoir. This means that each data bit was simultaneously written to six different nodes. Since only the current input was written in a single step, the reservoir is requested to have up to 10 short memory to fulfill the NARMA10 task.

We trained the output matrix using 2408 steps of training data with the least-squares method. The performance of reservoir computing was evaluated using NRMSE (normalized root-mean-square error) expressed by the following equation:

$$\text{NRMSE} = \sqrt{\frac{\sum_{s=1}^{N_{\text{test}}} (o_s - y_s)^2}{N_{\text{test}} \sigma^2(y_s)}}, \quad (7)$$

Fig. 7 Typical output result of reservoir computing with dipole-coupled nanomagnets. The solid and dotted lines show the output data of reservoir computing with trained matrix and the answer data with the NARMA10 function, respectively



where N_{test} is the number of test data, o_s and y_s are the output data and answer at step s , respectively, and $\sigma^2(y_k)$ is the variance of the answer.

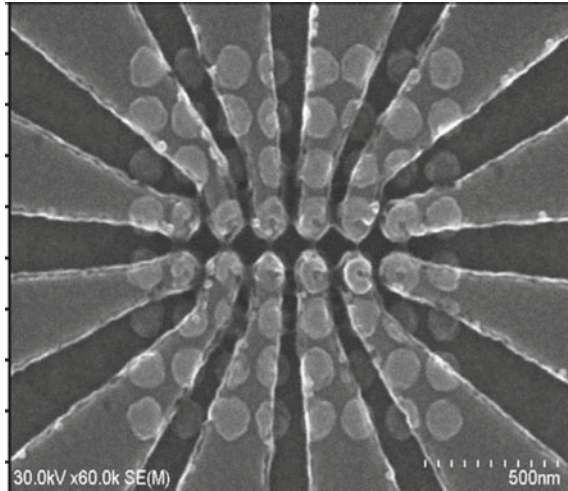
Figure 7 shows a typical output result of reservoir computing with dipole-coupled nanomagnets. The solid line shows the output data of reservoir computing with trained matrix and the dotted line shows the answer data with the NARMA10 function. The reservoir with the nanomagnet radius of 40 nm, the thickness of 10 nm, the nearest inter-dot distance of 10 nm, K_u of 0 or 20 kJ/m³, was used in Fig. 7. The output data of the trained reservoir computing show similar values as compared to the answer data. We calculated the NRMSE of the reservoir with 602 steps of the input data. The results show that the NRMSE between the output and answer data is 0.85, which is not low enough compared with those obtained by other methods. This is because the dipole-coupled nanomagnet reservoir used for the first trial (Fig. 6b) cannot hold sufficient old input values for the NARMA10 task. By changing the position of the node connected to the input layer and the updating procedure of the node state, the short-term memory capacity (Nomura et al. 2018) can be achieved with an NRMSE of 0.23 in the NARMA10 task with dipole-coupled nanomagnet reservoir (Zhu et al. 2018).

Figure 8 shows the SEM image of the prototype reservoir with dipole-coupled nanomagnets. The prototype reservoir comprises 8×8 nanomagnets with 2×2 contact holes. The distance between the nanomagnet of the prototypic reservoir was 12 nm. The micromagnetic simulations confirm that this structure can be used as a dipole-coupled nanomagnet reservoir.

5 Guiding Principle for the Future

We showed that the static magnetic moment vector in a dipole-coupled nanomagnet array behaves as a reservoir. The randomness of the inter-layer/inter-node coupling may enhance the performance of the magnetic reservoir. In the first trial, we randomly

Fig. 8 SEM image of the prototype reservoir



connected the input layer and the nodes in the reservoir. However, inter-node randomness was not utilized. Such randomness can be implemented by randomly changing the size and arrangement of the nanomagnets. Depending on the arrangement of the nanomagnets, the dipole-coupled nanomagnet array can behave as a spin glass or spin ice (Jensen et al. 2018). These arrangements can be used as a reservoir.

As described above, the MRAM reading/writing technology can be used to read the node state. Moreover, the inter-node connection using magnetic dipole coupling solves the wiring problem in realizing the hardware for RNN. The dipole-coupled nanomagnet reservoir, which is capable of creating interfaces with semiconductor technology by various existing technologies, is a candidate for practical use of physical reservoir computing. With the MRAM technology, one may fabricate giga-nodes class reservoir in principle. The guiding principle, however, to obtain better performance in a very large reservoir has not yet established. Nonetheless, explorations on the human brain class (21 giga-neurons) reservoir computing are not a dream.

Acknowledgments This work was supported by the Ministry of Internal Affairs and Communications, JAPAN.

References

- D.H. Ackley, G.E. Hinton, T.J. Sejnowski, A learning algorithm for boltzmann machines. *Cogn. Sci.* **9**(1), 147–169 (1985)
- D.J. Amit, H. Gutfreund, Spin-glass models of neural networks. *Phys. Rev. A* **32**(2), 1007–1018 (1985)
- L. Appeltant et al., Information processing using a single dynamical node as complex system. *Nat. Commun.* **2**, 468 (2011)

- A.F. Atiya, A.G. Parlos, New results on recurrent network training: unifying the algorithms and accelerating convergence. *IEEE Trans. Neural Netw.* **11**(3), 697–709 (2000)
- S. Bhatti et al., Spintronics based random access memory: a review. *Mater. Today* **20**(9), 530–548 (2017)
- R.P. Cowburn, M.E. Welland, Room temperature magnetic quantum cellular automata. *Science* **287**(5457), 1466–1468 (2000)
- N. Hikaru, N. Ryoichi, NAND/NOR logical operation of a magnetic logic gate with canted clock-field. *Appl. Phys. Express* **4**(1), (2011)
- N. Hikaru et al., Controlling operation timing and data flow direction between nanomagnet logic elements with spatially uniform clock fields. *Appl. Phys. Express* **10**(12), (2017)
- J.J. Hopfield, Neural networks and physical systems with emergent collective computational abilities. *Proc. Natl. Acad. Sci. USA-Biol. Sci.* **79**(8), 2554–2558 (1982)
- A. Imre et al., Majority logic gate for magnetic quantum-dot cellular automata. *Science* **311**(5758), 205–208 (2006)
- H. Jaeger, H. Haas, Harnessing nonlinearity: predicting chaotic systems and saving energy in wireless communication. *Science* **304**(5667), 78–80 (2004)
- J.H. Jensen, E. Folven, G. Tufte, Computation in artificial spin ice, in *The 2018 Conference on Artificial Life: A Hybrid of the European Conference on Artificial Life (ECAL) and the International Conference on the Synthesis and Simulation of Living Systems (ALIFE)* (2018), pp. 15–22
- T. Maruyama et al., Large voltage-induced magnetic anisotropy change in a few atomic layers of iron. *Nat. Nanotechnol.* **4**(3), 158–161 (2009)
- E.B. Myers et al., Current-induced switching of domains in magnetic multilayer devices. *Science* **285**(5429), 867–870 (1999)
- K. Nakajima et al., Information processing via physical soft body. *Sci. Rep.* **5**, 10487 (2015)
- H. Nomura et al., Reservoir computing with dipole-coupled nanomagnets (2018), [arXiv:1810.13140](https://arxiv.org/abs/1810.13140)
- A. Orlov et al., Magnetic quantum-dot cellular automata: recent developments and prospects. *J. Nanoelectron. Optoelectron.* **3**, 1–14 (2008)
- S.S.P. Parkin et al., Giant tunnelling magnetoresistance at room temperature with MgO (100) tunnel barriers. *Nat. Mater.* **3**(12), 862–867 (2004)
- S. Yuasa et al., Giant room-temperature magnetoresistance in single-crystal Fe/MgO/Fe magnetic tunnel junctions. *Nat. Mater.* **3**(12), 868–871 (2004)
- L. Zhu et al., Remarkable problem-solving ability of unicellular amoeboid organism and its mechanism. *R. Soc. Open Sci.* **5**(12) (2018)